Infrared investigation of the low-temperature structural and magnetic transitions in the spin-ladder candidate $(DT\text{-}TTF)_2Au(mnt)_2$

R. Wesołowski and J. T. Haraldsen
Department of Physics and Astronomy, University of Tennessee, Knoxville, Tennessee 37996, USA

J. L. Musfeldt
Department of Chemistry, University of Tennessee, Knoxville, Tennessee 37996, USA

T. Barnes
Department of Physics and Astronomy, University of Tennessee, Knoxville, Tennessee 37996, USA
and Physics Division, Oak Ridge National Laboratory, Oak Ridge, Tennessee 37831, USA

M. Mas-Torrent and C. Rovira
Institut de Ciéncia dels Materials de Barcelona, Campus de la U. A. B., E-08193 Bellaterra, Spain

R. T. Henriques and M. Almeida
Departamento de Quimica, ITN, P-2686 Sacaven Codex, Portugal

(Received 20 June 2003; revised manuscript received 12 August 2003; published 3 October 2003)

We report measurements of the variable temperature infrared response of the organic spin-ladder candidate dithiophentelrathiafulvalene gold maleonitrile dithiolate $[(DT\text{-}TTF)_2Au(mnt)_2]$. The 220 K structural transition is driven by massive symmetry breaking along the rung direction, whereas the 70 K magnetic transition is associated with a change in symmetry of the vibronically activated A_g modes in the rail direction. From molecular dynamics simulations, we assign the most important intramolecular vibrational modes involved in each transition. From an analysis of the charge-transfer behavior, we find that the localization of unpaired electrons in the interacting DT-TTF double chains is modified at these transition temperatures as well. To motivate future inelastic neutron-scattering studies, we have also calculated the spectrum of low-lying magnon excitations expected in this material, assuming an isotropic Heisenberg spin-ladder model. We estimate a gap of 0.6 meV for the one-magnon mode.

DOI: 10.1103/PhysRevB.68.134405 PACS number(s): 75.10.Pq, 78.68.+m, 33.20.Tp, 72.80.Le

I. INTRODUCTION

Quantum spin ladders have attracted considerable interest as intermediaries between one-dimensional (1D) chains and two-dimensional (2D) square lattices.[1–3] Additional interest has arisen from theoretical studies of the *t-J* model, which find that hole-doped spin-ladders can support superconductivity.[3,4] Thus, investigation of spin ladder materials allows a study of the relation between dimensionality and magnetic interactions, and may also lead to the identification of new families of high-T_c analog superconductors.[5] Whereas most ladder systems of current interest are structural ladders ($SrCu_2O_3$, $Sr_2Cu_3O_5$, $Cu14Sr_{24}O_{41}$, $CuCl_4MeCN$ and $[Ni(4,4'\text{-Bipy})_{2.5}(H_2O)_2] \times (ClO_4)_2 1.5(4,4'\text{-Bipy}) 2(H_2O)$,[1,4,6–8], several other ladderlike compounds are formed by the coupling of molecular building blocks. $(DT\text{-}TTF)_2Au(mnt)_2$,[2,9–12] $[Ph(NH_3)] \times (18\text{-crown-}6)[Ni(dmit)_2]$,[13] and $(5IAP)_2CuBr_4 2H_2O$ (Ref. 14–16) are three such examples. Of course, these materials should only be regarded as spin-ladder candidates, pending inelastic neutron scattering experiments.[17,18] $(DT\text{-}TTF)_2Au(mnt)_2$ and $(5IAP)_2CuBr_4 2H_2O$ are particularly attractive ladder candidates because they belong to families of compounds that share the same basic ladderlike structure, with tuneable magnetic properties depending on the nature of the counterion.[2,9–12,14–16] The fact that $(DT\text{-}TTF)_2Au(mnt)_2$ is an organic solid with delocalized charge and spin[2,9–12] brings additional features to an already fascinating area, which to date has been dominated by cuprates.[5]

$(DT\text{-}TTF)_2Au(mnt)_2$ is a semiconducting, organic charge-transfer salt formed from two building-block molecules, the donor DT-TTF (dithiophentetrathiafulvalene) and the acceptor $Au(mnt)_2$ (gold maleonitrile dithiolate).[2,9–12] The 300 K structure, shown in Fig. 1, is monoclinic. The *b* direction is defined by two columns of paramagnetic DT-TTF stacks, related by a screw axis and separated by one stack of diamagnetic $Au(mnt)_2$.[19] Note that this material is not a structural ladder; the molecular building blocks may, however, interact magnetically as a spin ladder, due to long-range intermolecular interactions. Since the spin resides on the DT-TTF molecule,[2,9–12] charge transfer occurs along the *b* direction. Because the DT-TTF stacks are dimerized, the charge transfer actually takes place between dimers; these interactions form the rails of the ladder. The rungs of the proposed ladder lie along the *c* direction and are formed by close $S \cdots S$ contacts between DT-TTF molecules from two adjacent stacks.[9,10,20] The rail and rung magnetic interaction strengths are estimated from susceptibility measurements to be $J_\parallel = 82$ K and $J_\perp = 142$ K;[2,9–12] their ratio $\alpha = J_\parallel / J_\perp \approx 0.6$ places $(DT\text{-}TTF)_2Au(mnt)_2$ in the theoretically inter-

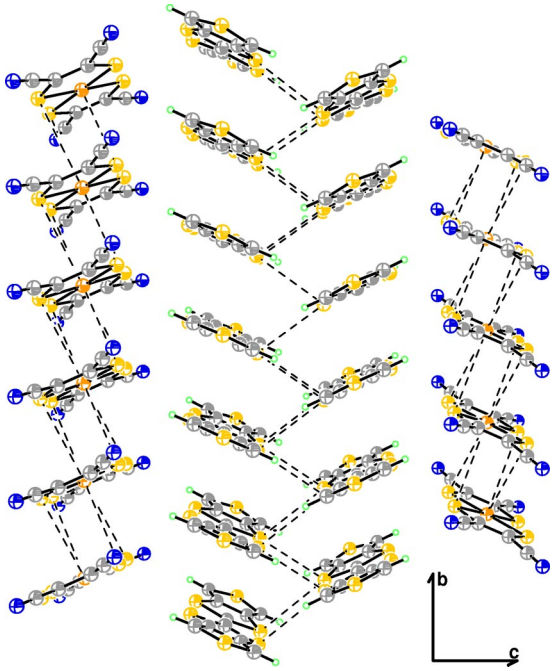

FIG. 1. The 300 K crystal structure of $(DT\text{-}TTF)_2Au(mnt)_2$. The *b* and *c* axes are the rail and rung orientations of the proposed spin ladder, respectively.

esting intermediate coupling regime.[21] μ^+SR (muon spin resonance) measurements suggest that there may, in addition, be significant interladder coupling.[12]

$(DT\text{-}TTF)_2Au(mnt)_2$ presents a transition at 220 K, observed in the dc resistivity and associated with a structural change and charge localization.[2,9–12] Below 70 K, both static and EPR (electron paramagnetic resonance) spin susceptibilities decrease exponentially toward zero, denoting the existence of a gap in the magnetic excitation spectrum.[2,9–12] The low-temperature quantum spin-liquid ground state, identified by μ^+SR measurements, is consistent with a two-leg spin-ladder model.[12]

In order to investigate the low-temperature transitions in $(DT\text{-}TTF)_2Au(mnt)_2$ we measured the variable-temperature infrared response. We find that the 220 K transition is due to symmetry breaking along the *c* direction, whereas at 70 K, another transition takes place, but only along *b*, and involves both the magnetic system as well as the vibronically activated A_g modes within the DT-TTF molecule. Dynamics simulations allow us to identify the most important modes for these transitions. In anticipation of future neutron-scattering experiments on $(DT\text{-}TTF)_2Au(mnt)_2$, we carried out calculations of the spectrum of low-lying magnetic excitations expected in this material, assuming a two-leg Heisenberg spin-ladder model.[21–23]

II. METHODS

A. Experimental techniques: Crystal growth and spectroscopy

Single crystals of the organic salt $(DT\text{-}TTF)_2Au(mnt)_2$ were obtained by electrocrystallization from a dichloromethane solution containing the donor and the tetrabutylammonium salt of $Au(mnt)_2^-$.[2,9–12] The resulting crystals were thin, opaque needles with typical dimensions of $\approx 3 \times 0.3 \times 0.1$ mm^3. Our measurements were carried out on the large (bc) crystal face. The needle direction of the crystal corresponds to *b*, and the perpendicular direction is the *c* axis.

Polarized infrared reflectance measurements were performed using a Bruker Equinox 55 Fourier-transform infrared spectrometer, equipped with a Bruker IRScope II infrared microscope. The spectral range was 600–15000 cm^{-1}, with 2 cm^{-1} resolution. Polarizers were used to separate the response along the *b* and *c* directions of the crystal. We investigated the spectra at 12 temperatures between 4 and 300 K, concentrating around the 70 K and 220 K transitions. The optical conductivity $\sigma_1(\omega)$ was calculated from the measured reflectance using a Kramers-Krönig analysis.[24] The charge-transfer band, in particular the decomposition of the complex shape and the changes in this shape with temperature, were determined by standard peak fitting techniques.[25]

B. Molecular dynamics calculations

We simulated the dynamics of $(DT\text{-}TTF)_2Au(mnt)_2$ using the commercially available program TITAN.[26] Because this material is a molecular solid, the calculations were carried out on isolated DT-TTF and $Au(mnt)_2$ building-block molecules to determine the response of the intramolecular modes, which dominate the middle infrared region.[2,9–12] The equilibrium geometry and vibrational modes of DT-TTF were evaluated with the parametrization method 3 semiempirical model, whereas the vibrational response of $Au(mnt)_2$ was calculated using a psuedopotential basis set of LACVP** and a density functional model, which was required for the integration of the orbital electrons of the heavy Au atomic center.[26] The vibrational response of the DT-TTF molecule was evaluated for both cationic $(+1)$ and neutral (0) cases which result from the sharing of one electron between two DT-TTF building blocks.[2,9–12] A group theory analysis, within the D_{2h} point group, allowed us to determine the number of expected vibrational modes and their respective symmetries for both the DT-TTF and $Au(mnt)_2$ building block molecules. For the DT-TTF molecule, we find $\Gamma_{vib} = 10A_g + 3B_{1g} + 9B_{2g} + 5B_{3g} + 4A_u + 9B_{1u} + 5B_{2u} + 9B_{3u}$, and for $Au(mnt)_2$, the modes are $\Gamma_{vib} = 8A_g + 3B_{1g} + 7B_{2g} + 3B_{3g} + 4A_u + 8B_{1u} + 4B_{2u} + 8B_{3u}$. The TITAN dynamics simulations provided both theoretical mode frequencies and corresponding symmetries. The symmetries were confirmed by visual inspection of the individual modes. Symmetry considerations were also used to identify modes that were expected to appear in the spectra. For instance, B_{1u}, B_{2u}, and B_{3u} modes are expected in the infrared due to their symmetry.[27,28] A_g modes may also be activated in the infrared due to electron-molecular coupling, an interaction that is expected in the *b*-polarized spectra of $(DT\text{-}TTF)_2Au(mnt)_2$.[27,28] All the features predicted from the dynamics calculations on the DT-TTF and $Au(mnt)_2$ building-block molecules were observed in the 300 K infrared spectra of $(DT\text{-}TTF)_2Au(mnt)_2$, but at low temperatures

this simple symmetry analysis does not fully capture the complexity of the observed spectra.

C. Predicted magnon spectrum

The magnon dispersion relations and density of states of $(DT\text{-}TTF)_2Au(mnt)_2$ were calculated assuming an $S=1/2$ two-leg Heisenberg antiferromagnetic spin-ladder model,[21,22] with $J_{\parallel}=82$, $J_{\perp}=142$ K, and $\alpha \approx 0.6$ taken from susceptibility measurements.[2,9–12] The Hamiltonian of this model is defined by

$$H=J_{\perp}\sum_{i=0}^{N} \vec{S}_{i,1}\cdot\vec{S}_{i,2}+\alpha(\vec{S}_{i,1}\cdot\vec{S}_{i+1,1}+\vec{S}_{i,2}\cdot\vec{S}_{i+1,2}). \quad (1)$$

The one-magnon dispersion relation $\omega(k)\equiv\omega_1(k)$ can be conveniently expressed as a Fourier series:[21]

$$\omega_1(k)=\sum_{l=0}^{\infty} a_l(\alpha)\cos(lk), \quad (2)$$

where the Fourier coefficients $a_l(\alpha)$ have been given analytically to fifth order in a power series expansion.[21] The two- and three-magnon continua are calculated by vector addition of the one-magnon excitations:

$$\omega_n(k)=\sum_{m=1}^{n} \omega_m(k), \quad (3)$$

where

$$k=\sum_{m=1}^{n} (k_m)[\mathrm{mod}(\pi)]. \quad (4)$$

Excluding bound modes, the minimum and maximum energy of the *n*-magnon continuum is evidently *n* times the magnitude of the one-magnon band minimum and maximum, respectively.[21] Density-of-states information can readily be generated using this construction as well.[21]

III. RESULTS AND DISCUSSION

A. Vibrational properties of $(DT\text{-}TTF)_2Au(mnt)_2$

1. 300 K infrared spectrum

Figure 2 displays the polarized infrared reflectance and calculated optical conductivity of $(DT\text{-}TTF)_2Au(mnt)_2$ at room temperature. The infrared spectra are anisotropic, with a different response in the two main directions. This kind of anisotropy, with a large charge-transfer band polarized along the donor stack direction and a low, flat response in the other orthogonal polarizations, is typical for low-dimensional semiconducting organic charge-transfer salts.[29–31] Along the *b* direction, the observed vibrational features have A_g symmetry. These modes are related to the motion of the DT-TTF building block molecule, and are activated by electron-molecular vibrational coupling.[27,28]. Along the *c* direction, we find normally infrared active B_{1u}, B_{2u}, and B_{3u} modes related to both DT-TTF and $Au(mnt)_2$ building-block molecules. Details of the assigned vibrational modes, based on a comparison of the spectra with our molecular dynamics simulations, are summarized in Table I. The table gives the experimental frequency of each peak in column 1, the theoretical frequency in column 2, the mode symmetry in column 3, the observed polarization in column 4, the low-temperature splitting in column 5, and a description of the molecular motion of each mode in column 6. As $\sigma_1(\omega) \rightarrow 0$ the result is in excellent agreement with the dc conductivity of $8\Omega^{-1}\mathrm{cm}^{-1}$.[10]

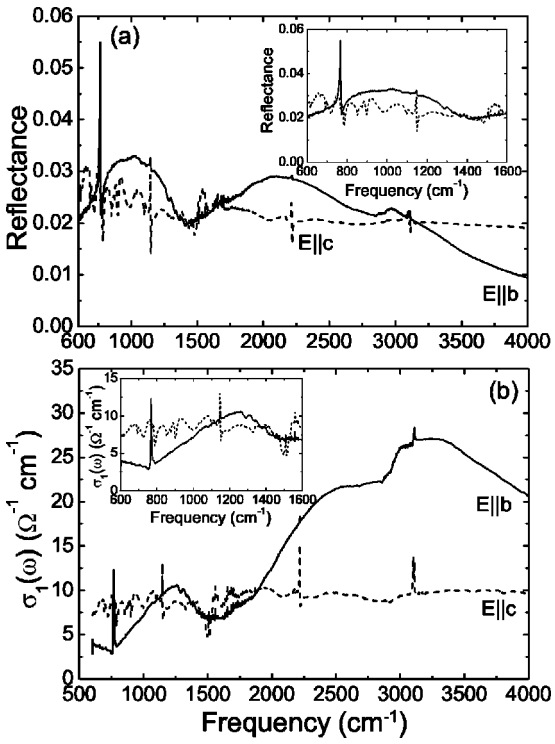

FIG. 2. 300 K polarized reflectance (a) and optical conductivity (b) of $(DT\text{-}TTF)_2Au(mnt)_2$. The insets show close-up views of the vibrational response.

2. Variable-temperature response along the b axis

Figure 3 shows the optical conductivity of $(DT\text{-}TTF)_2Au(mnt)_2$ in the rail direction at 4 and 300 K. There are significant modifications in the charge-transfer band with temperature. To quantify these changes, we fit the spectra with six model oscillators over the frequency range 1000–5500 cm^{-1} (inset, Fig. 3). The temperature dependence of the peak position and integrated area of these six oscillators is shown in Fig. 4. All oscillators soften at the 70 K transition, with only occasional changes at the 220 K transition.[32] Also notable are the trends in the two peaks around 3000 cm^{-1}, indicating that this splitting begins well above 300 K. Changes in the integral area of the largest peaks [Fig. 4(b)] are fairly substantial at the 70 K transition, although the trends are in different directions, indicating a redistribution of oscillator strength.

Figure 5 displays a closeup view of the variable-temperature infrared properties of $(DT\text{-}TTF)_2Au(mnt)_2$ in the *b* direction. The majority of these modes have A_g symmetry, activated by electron-molecular vibrational

TABLE I. Vibrational modes of $(DT\text{-}TTF)_2Au(mnt)_2$.

Experimental frequency (cm^{-1})	Theoretical frequency (cm^{-1})	Theoretical symmetry	Polarization	Low-temperature splitting	Molecular motion
697	712	B_{1u}	*c*	1:2	C—S bend DT-TTF
748	784	B_{1u}	*c*	1:2	C—S stretch; C═C rocking DT-TTF
767	810	A_g	*b*	1:20	C—S stretch DT-TTF
771	798	B_{2u}	*c*	1:2	C—S stretch; C═C rocking DT-TTF
818	812	B_{1u}	*c*	1:4	C—S stretch DT-TTF
870	869	B_{2u}	*c*	1:2	C—S stretch; C═C rocking $Au(mnt)_2$
885	885	B_{3u}	*c*	1:2	Out-of-plane rocking DT-TTF
924	964	B_{2u}	*c*	1:4	C—S stretch; C—C rocking DT-TTF
990	1016	B_{1u}	*c*		C—S; C═C stretch $Au(mnt)_2$
1027	1088	A_g	*b*	1:18	C—C; C—S stretch DT-TTF
1047	1088	B_{1u}	*c*	1:4	C—C; C—S stretch DT-TTF
1106	1124	B_{2u}	*c*	1:2	C—C rocking DT-TTF
1145	1157	B_{2u}	*c*	1:6	C—C stretch $Au(mnt)_2$; C═C rocking
1148	1157	B_{2u}	*b*		C—C stretch $Au(mnt)_2$; C═C rocking
1311	1409	A_g	*b*	1:12	C—C stretch DT-TTF
1339	1388	B_{1u}	*c*		C—C stretch DT-TTF
1387	1410	B_{1u}	*c*		C═C stretch $Au(mnt)_2$
1515	1655	A_g	*b*	1:20	C═C stretch DT-TTF
1652	1687	B_{2u}	*c*	1:3	C═C stretch; C—C rocking DT-TTF
2214	2231	B_{1u}	*c*		CN stretch $Au(mnt)_2$
3098	3113	B_{1u}	*c*	1:4	C═H stretch DT-TTF
3111	3114	A_g	*b*	1:4	C═H stretch DT-TTF

[a]All theoretical peaks have been assigned to experimental data.

[b]A_g modes of the DT-TTF molecule are infrared active due to electron-molecular vibrational coupling.

[c]Low-temperature splitting in the *b* direction is due to the 70 K transition, whereas low-temperature splitting in the *c* direction is due to the 220 K transition.

coupling,[27,28] and corresponding to molecular motions of the DT-TTF building-block molecule (Table I). These vibrational modes show clear low-temperature symmetry breaking; the splitting patterns are summarized in Table I. Of these various features, the $\sim 1{:}20$ (one peak splits into twenty) low-temperature splitting of the 780 cm^{-1} mode is the most striking [Fig. 5(a)]. Above 70 K, there is only one main peak,

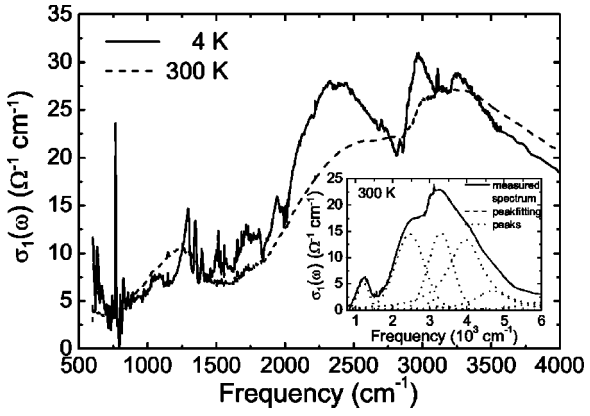

FIG. 3. Variable-temperature optical conductivity of $(DT\text{-}TTF)_2Au(mnt)_2$ polarized along the *b* direction. The inset shows a fit of the 300 K spectrum in the range of the charge-transfer band to several model Voight oscillators.

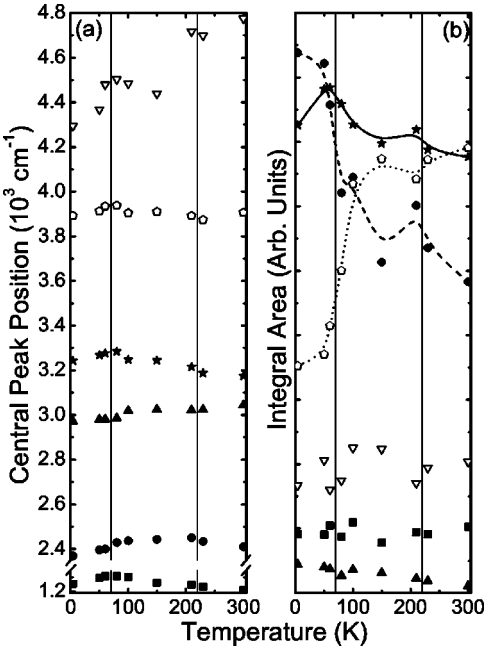

FIG. 4. Central peak positions (a) and integral areas (b) of the fitted oscillators in the charge-transfer band of $(DT\text{-}TTF)_2Au(mnt)_2$ as a function of temperature. Six oscillators were needed to capture the complex shape of the charge-transfer band. Selected lines guide the eye.

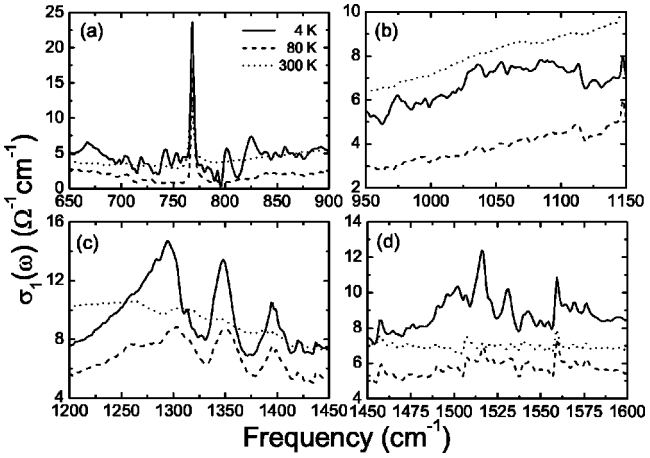

FIG. 5. Optical conductivity of selected vibrational modes of $(DT\text{-}TTF)_2Au(mnt)_2$ polarized along the *b* direction at 300, 80, and 4 K. (a) A_g mode (C—S stretching motion of DT-TTF), (b) A_g mode (C—C; C—S stretching motion of DT-TTF), (c) A_g mode (C—C stretching motion of DT-TTF), and (d) A_g mode (C═C stretching motion of DT-TTF).

but below the transition temperature the central peak is accompanied by numerous side peaks. The substantial low-temperature splitting of other vibronically activated A_g modes (1:18 for the 1027 cm^{-1} feature, 1:12 for the 1311 cm^{-1} mode, and 1:20 for the 1515 cm^{-1} feature) show that this effect is not restricted to a single mode. The other modes in Fig. 5 show similar trends, with the main changes occurring at the 70 K transition. We attribute a portion of low-temperature peak splitting to perturbations of the molecular motion resulting from site symmetry breaking. At the same time, x-ray scattering and μ^+SR measurements have shown that there are chain breaks that limit the effective length of the ladder in $(DT\text{-}TTF)_2Au(mnt)_2$ at low temperature.[2,9–12] These chain breaks, combined with symmetry breaking on the molecular site, can explain the observed vibrational splitting. Note that the *b*-polarized modes do not show any significant changes at the 220 K transition.

3. Variable-temperature response along the c axis

Figure 6 displays the optical conductivity of $(DT\text{-}TTF)_2Au(mnt)_2$ in the *c* direction (along the rungs of the proposed spin ladder) at 4 and 300 K. The spectra exhibit dramatic changes with temperature, with an explosion of new peaks below 220 K. A closeup view of this massive symmetry breaking is shown in Fig. 7. Between 600 and 1400 cm^{-1}, the symmetry breaking involving the C—C, C—S, and C═C motion is extraordinarily strong (with typically 1:2 or 1:4 peak splitting at 220 K, see Table I), whereas the splitting of the C—H stretch (1:4) at 3110 cm^{-1} is very weak, showing that most symmetry breaking takes place at the heart of the DT-TTF molecule. Note that all of the vibrational features in this polarization have B_{1u}, B_{2u}, or B_{3u} symmetry and correspond to normally infrared active modes, assigned as molecular motions of both DT-TTF and $Au(mnt)_2$ building-block molecules (Table I). There are no changes in *c*-polarized spectrum of $(DT\text{-}TTF)_2Au(mnt)_2$ at the 70 K transition.

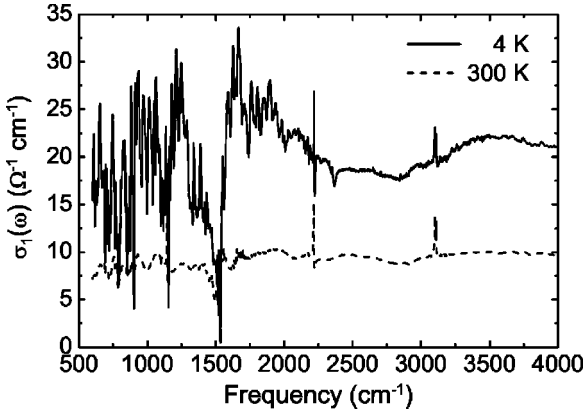

FIG. 6. Optical conductivity of $(DT\text{-}TTF)_2Au(mnt)_2$ polarized along the *c* direction at 300 and 4 K.

It is interesting that there are several *c*-polarized vibrational modes that are completely insensitive to the two low-temperature phase transitions in $(DT\text{-}TTF)_2Au(mnt)_2$. One of these features is at 2214 cm^{-1} [Fig. 7(c)] corresponding to CN stretching motion of $Au(mnt)_2$; this mode has B_{1u} symmetry. The insensitivity of the 2214 cm^{-1} CN stretching mode to temperature suggests that the outer portion of the $Au(mnt)_2$ building-block molecule is not involved in either the 220 K or 70 K transitions.[33] This observation, combined with the aforementioned symmetry breaking of DT-TTF-related modes, indicates that the 220 K transition is driven by a local distortion at the core of the $Au(mnt)_2$ building-block molecule combined with a massive distortion of the DT-TTF stack.

4. The 70 and 220 K phase transitions in $(DT\text{-}TTF)_2Au(mnt)_2$

The vibrational properties of $(DT\text{-}TTF)_2Au(mnt)_2$ provide microscopic information on the low temperature phase

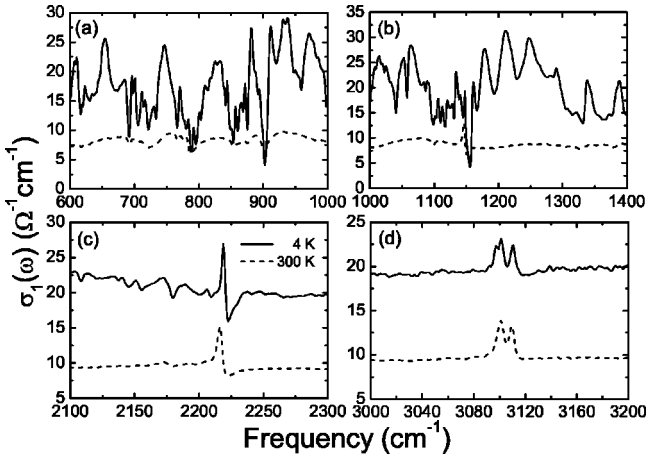

FIG. 7. Optical conductivity of selected vibrational modes of $(DT\text{-}TTF)_2Au(mnt)_2$ polarized along the *c* direction at 300 and 4 K. (a) B_{1u}, B_{2u}, and B_{3u} modes [various C—C; C═C; C—S motions of DT-TTF and $Au(mnt)_2$], (b) B_{1u} and B_{2u} modes [various C—C; C═C; C—S motions of DT-TTF and $Au(mnt)_2$], (c) B_{1u} mode (C—N stretching motion of $Au(mnt)_2$] and (d) B_{1u} mode [C—H stretching motion of $Au(mnt)_2$].

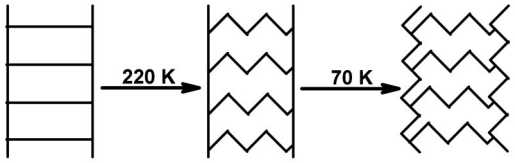

FIG. 8. Schematic view of the two low-temperature transitions of $(DT\text{-}TTF)_2Au(mnt)_2$, illustrating the symmetry breaking along the rungs (220 K) and rails (70 K) of the proposed spin ladder.

transitions in this material. Along the *b* direction, changes in the infrared spectrum appear only at 70 K. In contrast, only the *c*-polarized vibrational modes are sensitive to the 220 K transition. Thus, the 70 and 220 K transitions are mutually independent. Note that the deformation along *c* involves both DT-TTF and $Au(mnt)_2$ moieties, whereas changes in the *b* direction take place only within DT-TTF. Further, our dynamics simulations provide detailed information on the most important modes in each case. These results are summarized in Table I. Combining our results with previous dc resistivity and magnetic-susceptibility data,[2,9–12] we propose that the high-temperature transition at 220 K is a structural distortion that localizes charge along the *c* direction, whereas the 70 K transition is driven by both the magnetic system and a change in the A_g modes along *b*. Note that the energy scale of the latter is larger than is typical for magnetically driven transitions. A schematic diagram of these processes is shown in Fig. 8. Likewise, a similar scenario may explain the low-temperature transitions in other members of the $(DT\text{-}TTF)_2M(mnt)_2$ (M = Pt, Ni, Cu) family.

5. Comparison with other semiconducting organic charge-transfer salts

The low-temperature vibrational properties of $(DT\text{-}TTF)_2Au(mnt)_2$ are exceptionally rich, due to the striking mode splitting observed at the 220 and 70 K transitions. To illustrate how this kind of symmetry breaking is unusual for semiconducting organic charge-transfer salts, we compare our $(DT\text{-}TTF)_2Au(mnt)_2$ data with results on three other representative materials. Mode splitting in $(TMTSF)_2BF_4$ is driven by anion ordering,[34] low-temperature doublet spitting in $NPrQn(TCNQ)_2$ is due to a change in the charge distribution within the tetramer,[35] and the new low-temperature vibrational mode in β'-$(ET)_2CF_3CF_2SO_3$ is related to a spin-Peierls transition.[36] Although the nature of the mode splitting is entirely different in these model compounds, the symmetry breaking generally splits vibrational features into doublets or triplets. Thus, the symmetry breaking in $(DT\text{-}TTF)_2Au(mnt)_2$ is rather extraordinary.

B. Magnetic properties of $(DT\text{-}TTF)_2Au(mnt)_2$

Definitive confirmation that $(DT\text{-}TTF)_2Au(mnt)_2$ is a realization of the two-leg Heisenberg spin ladder will require inelastic neutron-scattering experiments, since neutron scattering is uniquely sensitive to the details of the effective magnetic interaction Hamiltonian at interatomic length scales. To assist future neutron-scattering studies of

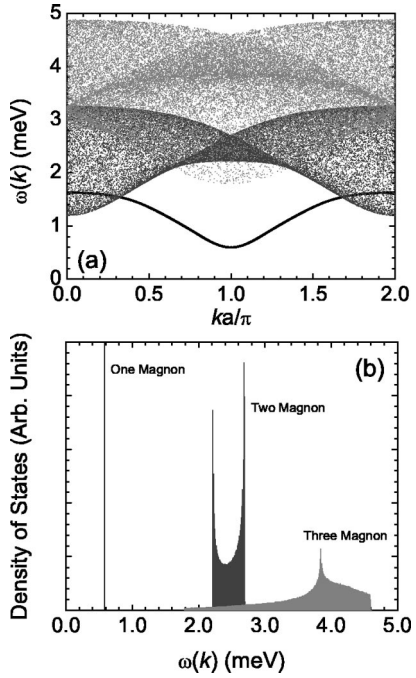

FIG. 9. (a) The one-magnon band and two- and three-magnon continua expected for $(DT\text{-}TTF)_2Au(mnt)_2$ in the two-leg Heisenberg ladder model, and (b) the density of states predicted in this model at $k=\pi/a$.

$(DT\text{-}TTF)_2Au(mnt)_2$, we have evaluated the spectrum of single-magnon excitations expected in this material, as well as the expected two- and three-magnon continua.

The calculated magnon spectra for $(DT\text{-}TTF)_2Au(mnt)_2$ are shown in Fig. 9(a). The minimum of the one-magnon band implies a gap of 0.6 meV at $k=\pi/a\approx 0.88$ Å^{-1}. Here, $a\approx 3.56$ Å is the distance between the rungs of the ladder. At the zone boundary, the one-magnon energy is 1.6 meV. The two-magnon continuum has a minimum and maximum of 1.2 meV and 3.2 meV, respectively, and the three-magnon continuum covers the range 1.8 to 4.8 meV. Note that the two-magnon continuum is predicted to cross under the one-magnon band at small k, so for $ka/\pi \lesssim 0.3$, the lowest-lying excitations are two-magnon states. There is a similar crossover of the two- and three-magnon continua in the region $0.7 \lesssim ka/\pi \lesssim 1.3$; in this region, the lower boundary of the three-magnon continuum lies below the two-magnon continuum. This crossover is also evident in the density of states at $k=\pi/a$, which is shown in Fig. 9b. Another interesting feature of these higher excitations in $(DT\text{-}TTF)_2Au(mnt)_2$ is a ''folding'' of the two-magnon continuum, which leads to a singularity in the density of states within the continuum near $k=\pi/a$; this twisting is also evident in Fig. 9(a). Finally, we note that two-magnon bound states with $S_{tot}=0$ and $S_{tot}=1$ are also predicted by the spin-ladder model,[37] and may be observed using Raman[38] and inelastic neutron scattering, respectively. Although these higher excitations would normally be quite difficult to observe, the rather large value of α in $(DT\text{-}TTF)_2Au(mnt)_2$ may allow observation of some part of these higher magnetic continua.

IV. CONCLUSIONS

We report the variable-temperature polarized infrared properties of the organic spin ladder candidate $(DT\text{-}TTF)_2Au(mnt)_2$ in order to investigate the 220 and 70 K transitions. Complementary dynamics simulations allow us to identify the most important vibrational modes associated with each distortion. The 220 K transition is driven by massive symmetry breaking along the *c* axis. Evidence for a new transition at 70 K is also observed and is associated with a change in both magnetic and vibrational properties in the *b* direction. The charge-transfer bands, which are connected with the localization of unpaired electrons in the interacting DT-TTF double chains, are modified at the lower transition temperature as well. It has been suggested that the magnetic interactions along the *b* (rail) and *c* (rung) directions in $(DT\text{-}TTF)_2Au(mnt)_2$ might be an accurate realization of the two-leg Heisenberg spin ladder. Future inelastic neutron-scattering measurements should allow an unambiguous test of this hypothesis. To assist in planning such a study, we have given numerical results for the spectrum of single-magnon excitations expected in this material, as well as the envelopes of the two- and three-magnon continua assuming a Heisenberg spin-ladder model. We estimate a one-magnon gap of 0.6 meV at $k \approx 0.88$ Å^{-1}.

ACKNOWLEDGMENTS

This project was supported at the University of Tennessee by the Division of Materials Research at the National Science Foundation (Grant No. DMR-01394140. Work in Barcelona was supported by DGI-Spain (Grant No. BQU2000-1157) and DURSI-Catalunya (Grant No. 2001SGR-00362) and in Portugal by FCT under Contract POCTI/35342/QUI/2000). The European collaboration was supported by EU COST Action D14/0003/99. We thank J.D. Woodward for the structural rendering of $(DT\text{-}TTF)_2Au(mnt)_2$ and for useful conversations.

[1] E. Dagotto and T.M. Rice, Science **271**, 618 (1996).
[2] C. Rovira, *Structure and Bonding*, edited by J. Veciana (Springer, Berlin 2001), Vol. 100, pp. 163–188.
[3] E. Dagotto, Rep. Prog. Phys. **62**, 1525 (1999).
[4] S. Maekawa, Science **273**, 1515 (1996).
[5] T.M. Rice, S. Gopalan, and M. Sigrist, Europhys. Lett. **23**, 445 (1993).
[6] M. Azuma, Z. Hiroi, M. Takano, K. Ishida, and Y. Kitaoka, Phys. Rev. Lett. **73**, 3463 (1994).
[7] B.R. Patyal, B.L. Scott, and R.D. Willett, Phys. Rev. B **41**, 1657 (1990).
[8] O. Yahgi, H. Li, and T.L. Groy, Int. Ophthalmol. **36**, 4292 (1997).
[9] E. Ribera, C. Rovira, J. Veciana, J. Tarrs, E. Canadell, R. Rousseau, E. Molins, M. Mas, J.-P. Schoeffel, J.-P. Pouget, J. Morgado, R.T. Henriques, and M. Almeida, Chem.-Eur. J. **5**, 2025 (1999).
[10] C. Rovira, J. Veciana, E. Ribera, J. Tarrs, E. Canadell, R. Rousseau, M. Mas, E. Molins, M. Almeida, R.T. Henriques, J. Morgado, J.-P. Schoeffel, and J.-P. Pouget, Angew. Chem., Int. Ed. Engl. **36**, 2324 (1997).
[11] E. Ribera, C. Rovira, J. Veciana, J. Tarrés, E. Candell, R. Rousseau, E. Molins, M. Mas, J.-P. Schoeffel, J.-P. Pouget, J. Morgado, V. Gama, R.T. Henriques, and M. Almeida, Synth. Met. **102**, 1743 (1999).
[12] D. Arčon, A. Lappas, S. Margadonna, K. Prassides, E. Ribera, J. Veciana, C. Rovira, R.T. Henriques, and M. Almeida, Phys. Rev. B **60**, 4191 (1999).
[13] S. Nishihara, T. Akutagawa, T. Hasegawa, and T. Nakamura, Chem. Commun. (Cambridge) **2002**, 408 (2002).
[14] T. Matsumoto, Y. Miyazaki, A.S. Albrecht, C.P. Landee, M.M. Turnbull, and M. Sorai, J. Phys. Chem. B **104**, 9993 (2000).
[15] C.P. Landee, M.M. Turnbull, C. Galeriu, J. Giantsidis, and F.M. Woodward, Phys. Rev. B **63**, 100402 (2001).
[16] F.M. Woodward, A.S. Albrecht, C.M. Wynn, C.P. Landee, and M.M. Turnbull, Phys. Rev. B **65**, 144412 (2002).
[17] A.W. Garrett, S.E. Nagler, T. Barnes, and B.C. Sales, Phys. Rev. B **55**, 3631 (1997).
[18] Unlike the measurements of bulk properties, inelastic neutron scattering directly measures the dispersion relations of individual magnetic excitations that allow analysis of the interactions between ions assumed in a model magnetic Hamiltonian.
[19] The unit cell consists one DT-TTF molecule and 0.5 $Au(mnt)_2$ molecules (Ref. 10).
[20] C. Rovira, J. Veciana, N. Santaló, J. Tarrés, J. Cirujeda, E. Molinis, J. Liorca, and E. Espinosa, J. Org. Chem. **59**, 3307 (1994).
[21] T. Barnes, Phys. Rev. B **67**, 024412 (2003).
[22] T. Barnes, E. Dagotto, J. Riera, and E.S. Swanson, Phys. Rev. B **47**, 3196 (1993).
[23] T. Barnes and J. Riera, Phys. Rev. B **50**, 6817 (1994).
[24] F. Wooten, *Optical Properties of Solids* (Academic Press, New York, 1972).
[25] We used Voight oscillators in the fitting precedure.
[26] Wavefunction Inc., Schrodinger Inc., TITAN© (1999).
[27] M.J. Rice, Phys. Rev. Lett. **37**, 36 (1976).
[28] M.J. Rice, V.M. Yartsev, and C.S. Jacobsen, Phys. Rev. B **21**, 3437 (1980).
[29] D.B. Tanner, in *Extended Linear Chain Compounds*, Optical Properties of 1D Systems Vol. 2, edited by J. S. Miller (Plenum Publishing Corp, New York, 1982), Chap. 5.
[30] C.S. Jacobsen, in *Semiconductors and Semimetals*, Optical Properties Vol. 27, edited by E.M. Conwell (Academic Press, New York, 1985), Chap. 5.
[31] V.M. Yartsev and R. Świetlik, Rev. Solid State Sci. **4**, 69 (1990).
[32] We regard the 4600 cm^{-1} mode as least reliable, as it is merely simulates the tail of the charge transfer feature.
[33] Examination of the low-temperature splitting data in Table I shows that the majority of modes that do not display low-temperature symmetry breaking are related to the motion of $Au(mnt)_2$.
[34] C.C. Homes and J.E. Eldridge, Phys. Rev. B **42**, 9522 (1990).
[35] J.L. Musfeldt, K. Kamarás, and D.B. Tanner, Phys. Rev. B **45**, 10197 (1992).

[36] R. Wesołowski, I. Olejniczak, and J. A. Schlueter (unpublished); R. Wesołowski, Masters thesis, Poznań University of Technology, Poland, 2002 (unpublished).

[37] W. Zheng, C.J. Hamer, and R.R.P. Singh, cond-mat/0211346 (unpublished).

[38] P.A. Fleury and R. Loudon, Phys. Rev. **166**, 514 (1968).